THE REMARKABLE AFTERGLOW OF GRB 061007: IMPLICATIONS FOR OPTICAL FLASHES AND GRB FIREBALLS

C. G. Mundell,[1] A. Melandri,[1] C. Guidorzi,[1,2,3] S. Kobayashi,[1] I. A. Steele,[1] D. Malesani,[4] L. Amati,[5]
P. D'Avanzo,[3,6] D. F. Bersier,[1] A. Gomboc,[1,7] E. Rol,[8] M. F. Bode,[1] D. Carter,[1] C. J. Mottram,[1]
A. Monfardini,[1,9] R. J. Smith,[1] S. Malhotra,[10] J. Wang,[11] N. Bannister,[8]
P. T. O'Brien,[8] and N. R. Tanvir[8]

ABSTRACT

We present a multiwavelength analysis of *Swift* GRB 061007. The 2 m robotic Faulkes Telescope South began observing 137 s after the onset of the γ-ray emission, when the optical counterpart was already decaying from $R \sim 10.3$ mag, and continued observing for the next 5.5 hr. These observations begin during the final γ-ray flare and continue through and beyond a long, soft tail of γ-ray emission whose flux shows an underlying simple power-law decay identical to that seen at optical and X-ray wavelengths, with temporal slope $\alpha \sim 1.7$ ($F \propto t^{-\alpha}$). This remarkably simple decay in *all* of these bands is rare for *Swift* bursts, which often show much more complex light curves. We suggest the afterglow emission begins as early as 30–100 s and is contemporaneous with the ongoing variable prompt emission from the central engine, but originates from a physically distinct region dominated by the forward shock. The observed multiwavelength evolution of GRB 061007 is explained by an expanding fireball whose optical, X-ray, and late-time γ-ray emission is dominated by emission from a forward shock with typical synchrotron frequency, ν_m, that is already below the optical band as early as $t = 137$ s and a cooling frequency, ν_c, above the X-ray band to at least $t = 10^5$ s. In contrast, the typical frequency of the reverse shock lies in the radio band at early time. We suggest that the unexpected lack of bright optical flashes from the majority of *Swift* GRBs may be explained with a low ν_m originating from small microphysics parameters, ϵ_e and ϵ_B. Finally, the optical light curves imply a minimum jet opening angle $\theta = 4.7°$, and no X-ray jet break before $t \sim 10^6$ s makes GRB 061007 a secure outlier to spectral energy correlations.

Subject headings: cosmology: observations — gamma rays: bursts — radiation mechanisms: nonthermal — shock waves

1. INTRODUCTION

Gamma-ray bursts (GRBs) are the most instantaneously luminous cosmological objects known, and although their transient nature makes them observationally challenging to follow up at other wavelengths after the initial burst of γ rays, their brightness and large redshift range ($0.0085 < z < 6.29$) ensure they remain uniquely useful as probes of the early universe. With the launch of the GRB-dedicated *Swift* satellite (Gehrels et al. 2004), early-time monitoring of the radiation from GRBs across the electromagnetic spectrum is now possible. Rapid and accurate localization of GRBs and immediate dissemination of their positions drive ground-based follow-up campaigns with small and large optical and infrared robotic telescopes such as ROTSE, REM, the Liverpool and Faulkes Telescopes, while *Swift*'s onboard narrow field instruments the X-Ray Telescope (XRT) and the Ultraviolet Optical Telescope (UVOT) observe a large fraction of GRBs within minutes of their detection with the Burst Alert Telescope (BAT).

Following the detection of a very bright optical counterpart to GRB 990123 by ROTSE (Akerlof et al. 1999) contemporaneous with the γ-ray emission and consistent with models predicting optical emission from a reverse shock in the relativistic outflow (Sari & Piran 1999; Kobayashi & Sari 2000; Kobayashi 2000; Nakar & Piran 2005), there was strong anticipation of routine detection of optical flashes at early times with UVOT, which can detect optical emission below the detection threshold of ROTSE. However, despite rapid and accurate localization of γ-ray emission and subsequent follow-up by UVOT, bright optical flashes remain elusive (Roming et al. 2006). In some cases, the high redshift of the burst renders it undetectable due to the lack of UVOT filters redder than V band (i.e., $z > 4$); in others, intrinsic faintness coupled with local extinction pushes the OT below the detection threshold of the UVOT (Oates et al. 2006). Ground-based observations from large robotic telescopes, optimized for the rapid follow-up of GRB alerts (Guidorzi et al. 2005, 2006; Dai et al. 2007), are increasing the number of well-sampled, early-time multicolor optical light curves over a wide range of magnitudes (Gomboc et al. 2007; Melandri et al. 2007) and revealing more complex decays than expected from pre-Swift light curves (Guidorzi et al. 2005; Stanek et al. 2007; Dai et al. 2007; Monfardini et al. 2006; Oates et al. 2006). Small departures from a power-law decay (i.e., $\Delta m \lesssim 0.5$ mag) are interpreted as interactions between the expanding fireball and dense clumps in the circumburst medium (Lazzati et al. 2002; Heyl & Perna 2003; Nakar et al. 2003;

[1] Astrophysics Research Institute, Liverpool John Moores University, Birkenhead CH41 1LD, UK.

[2] Dipartimento di Fisica, Universitá di Milano-Bicocca, Milan 20126, Italy.

[3] INAF−Osservatorio Astronomico di Brera, Merate (LC) 23807, Italy.

[4] International School for Advanced Studies (SISSA-ISAS), Trieste 34014, Italy.

[5] INAF-IASF Bologna, Bologna, Italy.

[6] Università dell'Insubria, Dipartimento di Fisica e Matematica, Como I-22100, Italy.

[7] FMF, University in Ljubljana, Ljubljana 1000, Slovenia.

[8] Department of Physics and Astronomy, University of Leicester, University Road, Leicester LE1 7RH, UK.

[9] CNRS-CTBT, Grenoble 38000, France.

[10] School of Earth and Space Exploration, Arizona State University, Tempe, AZ 85287-1404.

[11] Center for Astrophysics, University of Science and Technology of China, Hefei, Anhui 230026, China.

Guidorzi et al. 2005), while major rebrightenings suggest late-time energy injections (Kumar & Piran 2000; Sari & Mészáros 2000; Zhang & Mészáros 2002; Stanek et al. 2007; Wozniak et al. 2006; Monfardini et al. 2006); bright optical flares consistent with reverse shocks, however, are still rare or unconfirmed (Boër et al. 2006; Jelínek et al. 2006). Complex light curves are now common at X-ray energies with *Swift* light curves revealing a canonical shape comprising a "three-segment" structure inconsistent with a single power-law decay, with X-ray flares superimposed in at least 50% of bursts. Such complexity has been a major surprise of the *Swift* era and has led to a general acceptance of longlived activity (Burrows et al. 2005; O'Brien et al. 2006), challenging standard central engine models. A significant minority of GRB X-ray light curves show a fairly smooth decay consistent with an afterglow at early time (O'Brien et al. 2006) but most of these cases lack simultaneous optical data sufficient to fully test current models.

Here we present multicolor $BVRi'$ light curves of the very bright optical counterpart to GRB 061007 obtained automatically by the 2 m robotic telescope, the Faulkes Telescope South (FTS) at Siding Spring, Australia which began observing 137 s after the onset of the γ-ray emission when the optical counterpart was already decaying from $R \sim 10.3$ mag, and continued observing for the next 5.5 hr.[12] We show that GRB 061007 is unusual for a *Swift* burst in that it shows a remarkably simple power-law decay from γ rays to optical wavelengths. Its isotropic equivalent radiated energy is one of the highest ever measured ($E_{\rm iso} \sim 10^{54}$ ergs) and its peak νF_ν energy, $E_{\rm peak}$, is well determined. It therefore provides a useful test of current spectral energy correlations without the complication of highly structured light curves (Amati et al. 2002; Ghirlanda et al. 2004; Liang & Zhang 2005; Firmani et al. 2006; Amati 2006).

The multiwavelength observations and analyses are presented in § 2; results and discussion are presented in § 3, where a shock model is proposed to explain the observed multiwavelength evolution and broadband spectral energy distribution. We consider implications for cosmological spectral energy correlations and present our conclusions in § 4. Throughout, 1 σ errors are given unless otherwise stated.

2. OBSERVATIONS AND ANALYSIS

On 2006 October 07, 10:08:08 UT[13] *Swift*-BAT detected GRB 061007 (trigger 232683) at coordinates R.A. $= 03^{\rm h}05^{\rm m}16^{\rm s}$, decl. $= -50°29'15''$ (J2000.0; 3' 90% containment radius). The prompt emission from GRB 061007 was also detected at MeV energies by Konus-*Wind* (20 keV–10 MeV) (Golenetskii et al. 2006), *Suzaku* WAM (50 keV–5 MeV) (Yamaoka et al. 2006), and *RHESSI* (20 keV–10 MeV) (Wigger et al. 2006), whose detections provide estimates of the peak energy $E_{\rm peak}$ of 399^{+19}_{-18} keV (Golenetskii et al. 2006), 561^{+29}_{-27} keV (Yamaoka et al. 2006), and 391^{+58}_{-52} keV (Wigger et al. 2006), respectively. The *Swift* BAT γ-ray light curve shows three significant flat-topped peaks with substantial substructure, and a small fourth peak (from $t_0 + 75$ s) that shows long exponential decay and faint emission detectable to $t \sim 900$ s (Markwardt et al. 2006; Schady et al. 2006b). The fluence, $S_\gamma = 2.49 \times 10^{-4}$ ergs cm^{-2}, measured by Konus-*Wind*, corresponds to an isotropic equivalent energy $E_{\rm iso} \sim 10^{54}$ ergs (Golenetskii et al. 2006) for the spectroscopic redshift $z = 1.261$

[12] Observations obtained as part of the RoboNet-1.0 project: http://www.astro.livjm.ac.uk/RoboNet.

[13] Throughout the paper $t = 0$.

TABLE 1
FTS, VLT AND MAGELLAN OPTICAL OBSERVATIONS OF GRB 061007

Telescope	Δt (minute)	Filter	Exposure Time (s)	Magnification $\pm$ Error[a]
FTS..........	2.28	$R_{\rm C}$	10.0	10.34 ± 0.11
	2.63	$R_{\rm C}$	10.0	10.68 ± 0.12
	3.00	$R_{\rm C}$	10.0	10.96 ± 0.11
	4.63	B	10.0	12.81 ± 0.20
	5.52	V	10.0	12.52 ± 0.20
	6.38	SDSS i'	10.0	11.67 ± 0.04
	7.50	B	30.0	13.56 ± 0.10
	8.80	$R_{\rm C}$	30.0	12.85 ± 0.10
	12.25	SDSS i'	30.0	13.03 ± 0.04
	16.73	B	60.0	15.18 ± 0.09
	18.42	$R_{\rm C}$	60.0	14.28 ± 0.10
	20.18	SDSS i'	60.0	13.90 ± 0.11
	21.93	B	120.0	15.64 ± 0.07
	24.63	$R_{\rm C}$	120.0	14.78 ± 0.08
	27.38	SDSS i'	120.0	14.47 ± 0.10
	30.15	B	180.0	16.24 ± 0.09
	33.78	$R_{\rm C}$	180.0	15.36 ± 0.08
	37.55	SDSS i'	180.0	15.04 ± 0.09
	41.45	B	120.0	16.70 ± 0.09
	44.08	$R_{\rm C}$	120.0	15.71 ± 0.08
	46.83	SDSS i'	120.0	15.31 ± 0.10
	49.63	B	180.0	16.92 ± 0.10
	53.28	$R_{\rm C}$	180.0	15.98 ± 0.07
	57.07	SDSS i'	180.0	15.59 ± 0.09
	60.85	B	240.0	17.27 ± 0.11
	68.40	$R_{\rm C}$	30.0	16.25 ± 0.09
	70.50	B	10.0	17.48 ± 0.11
	71.23	V	10.0	17.16 ± 0.21
	72.13	SDSS i'	10.0	15.94 ± 0.11
	73.17	B	30.0	17.66 ± 0.13
	74.40	$R_{\rm C}$	30.0	16.48 ± 0.09
	75.62	SDSS i'	30.0	16.06 ± 0.10
	76.90	B	60.0	17.66 ± 0.20
	78.53	$R_{\rm C}$	60.0	16.59 ± 0.09
	80.32	SDSS i'	60.0	16.15 ± 0.10
	82.08	B	120.0	17.78 ± 0.18
	84.77	$R_{\rm C}$	120.0	16.72 ± 0.09
	87.52	SDSS i'	120.0	16.30 ± 0.09
	90.30	B	180.0	17.92 ± 0.16
	93.95	$R_{\rm C}$	180.0	16.95 ± 0.09
	97.73	SDSS i'	180.0	16.51 ± 0.10
	101.55	B	120.0	18.18 ± 0.17
	104.20	$R_{\rm C}$	120.0	17.03 ± 0.08
	106.93	SDSS i'	120.0	16.63 ± 0.10
	109.68	B	180.0	18.36 ± 0.14
	113.43	$R_{\rm C}$	180.0	17.26 ± 0.08
	117.20	SDSS i'	180.0	16.87 ± 0.11
	120.98	B	240.0	18.67 ± 0.17
	125.62	$R_{\rm C}$	240.0	17.50 ± 0.15
	145.55	$R_{\rm C}$	300.0	17.55 ± 0.11
	150.92	$R_{\rm C}$	300.0	17.65 ± 0.10
	160.12	V	450.0	18.38 ± 0.18
	171.98	B	450.0	19.25 ± 0.15
	191.77	SDSS i'	300.0	17.57 ± 0.13
	197.15	SDSS i'	300.0	17.63 ± 0.12
	203.75	$R_{\rm C}$	300.0	18.19 ± 0.11
	209.13	$R_{\rm C}$	150.0	18.20 ± 0.11
	215.67	V	600.0	18.90 ± 0.17
	242.75	B	300.0	19.62 ± 0.20
	249.33	SDSS i'	300.0	18.17 ± 0.13
	254.72	SDSS i'	300.0	18.17 ± 0.12
	261.28	$R_{\rm C}$	600.0	18.95 ± 0.13
	273.20	V	600.0	19.38 ± 0.20
	295.43	B	600.0	20.09 ± 0.26

TABLE 1—*Continued*

Telescope	Δt (minute)	Filter	Exposure Time (s)	Magnification ± Error[a]
	307.42	SDSS i'	600.0	18.39 ± 0.15
	319.37	R_C	300.0	19.20 ± 0.25
	331.28	V	300.0	19.99 ± 0.30
VLT	899.58	R_C	600.0	21.48 ± 0.03
Magellan...	2494.80	R_C	240.0	23.65 ± 0.50
	4086.64	R_C	240.0	>23.30

[a] Quoted errors for BVi' filters are statistical. Absolute calibration requires inclusion of the systematic error 0.25 mag due to the uncertainty in the USNO B1 photometric calibration. This error has been fully included when deriving the SED (see Fig. 2 and Table 3).

(Osip et al. 2006; Jakobsson et al. 2006). The *Swift* XRT and UVOT began observing 80 s after the BAT trigger time and identified a very bright X-ray/optical counterpart with a rapid decay rate $\alpha_X = 1.6 \pm 0.1$ ($F \propto t^{-\alpha}$) (Schady et al. 2006a; Vetere et al. 2006; Schady & Pandy 2006b).

Robotically triggered photometric observations with ground-based telescopes ROTSE and the FTS began at 26 and 137 s, respectively, each identifying the optical counterpart with brightnesses 13.6 mag (unfiltered) (Rykoff et al. 2006) and 10.3 mag (R band) (Mundell et al. 2006; Bersier et al. 2006), respectively, at R.A. = $03^h05^m19.56^s$, decl. = $-50°30'2.6''$ ($\pm1.2''$) (J2000.0). After taking the initial 3×10 s exposure R-band images, the FTS continued to observe for the next 5.5 hr, cycling through BRi' filters with V imaging interspersed and using increasing exposure times, until finishing with a 300 s V-band image at UT = 15:39:25.322. Initial photometric calibration was performed with GAIA (Optimal PSF Photometry Tool) relative to all the catalogued stars (USNO B1 and NOMAD) in the $4.6' \times 4.6'$ field of view and the bright star near the OT (R.A. = $03^h05^m23.5^s$, decl. = $-50°30'16.6''$) was used for point-spread function (PSF) determination. A 5×120 s R-band image was also acquired using FORS1 on the VLT at 2006 October 8.04702 UT (0.6247 days after the burst); the observing conditions were photometric and calibration was performed relative to Landolt standard stars. The

FTS R band were adjusted to the VLT photometry to provide a well-calibrated R-band light curve. Later time R-band images were acquired with the IMACS instrument on the Magellan-I Baade Telescope at Las Campanas Observatory on October 9 and 10 and calibrated with respect to the VLT image. Finally, magnitudes are corrected for Galactic extinction: from $E_{B-V} = 0.020$ (Schlegel et al. 1998), and $A_V = R_V \times E_{B-V} = 0.06$ mag, with $R_V = 3.1$, we evaluated the extinction in the other filters following Cardelli et al. (1989): $A_B = 0.08$ mag, $A_R = 0.05$ mag, and $A_{i'} = 0.04$ mag. Fluxes were derived following Fukugita et al. (1996), and calibration uncertainties for the remaining FTS filters, which do not affect the overall light curve properties, were taken into account when deriving the broadband spectral energy distribution. Results are summarized in Table 1 and plotted in Figure 1 along with the mask-tagged background-subtracted BAT light curve, which was produced by the standard BAT pipeline (HEADAS ver. 6.1.1). The BAT light curve was masked with the ground-refined coordinates provided by the BAT team (Markwardt et al. 2006). BAT spectra have been corrected for systematics with the `batphasyserr` tool and the original 80 energy channels have been grouped to have 3 σ significant grouped channels. We processed XRT data from 200 to 400 s after the trigger adopting standard screening and we extracted the XRT 0.3–10 keV spectrum: data were in Window Timing (WT) mode and the average count rate was below 100 counts s^{-1} so that no correction for pile up was required (Romano et al. 2006).

The brightness of the burst and the similarity of the decay rate in all bands (see Fig. 1 and Table 2) allows the construction of an early-time broadband spectral energy distribution (SED), shown in Figure 2. The joint XRT/BAT 0.3–150 keV spectrum from 200 to 400 s is well fit with a power law with significant absorption in excess of the Galactic, N_H(Gal) = 1.75×10^{20} cm^{-2} (Kalberla et al. 2005), such that $\beta_{X-\gamma} = 1.01 \pm 0.03$ ($F \propto \nu^{-\beta}$) and rest-frame $N_H = (5.8 \pm 0.4) \times 10^{21}$ cm^{-2} (90% confidence level). As shown in Figure 2 and Table 3, when β is free to vary, the best fit is obtained for $\beta_{opt-X-\gamma} = 1.02 \pm 0.05$ and $A_V = 0.48 \pm 0.19$ mag with an SMC-like extinction profile (Pei 1992). Figure 3 shows the BAT (15–350) light curve and the evolution of the hardness ratio derived from a comparison of the count rates
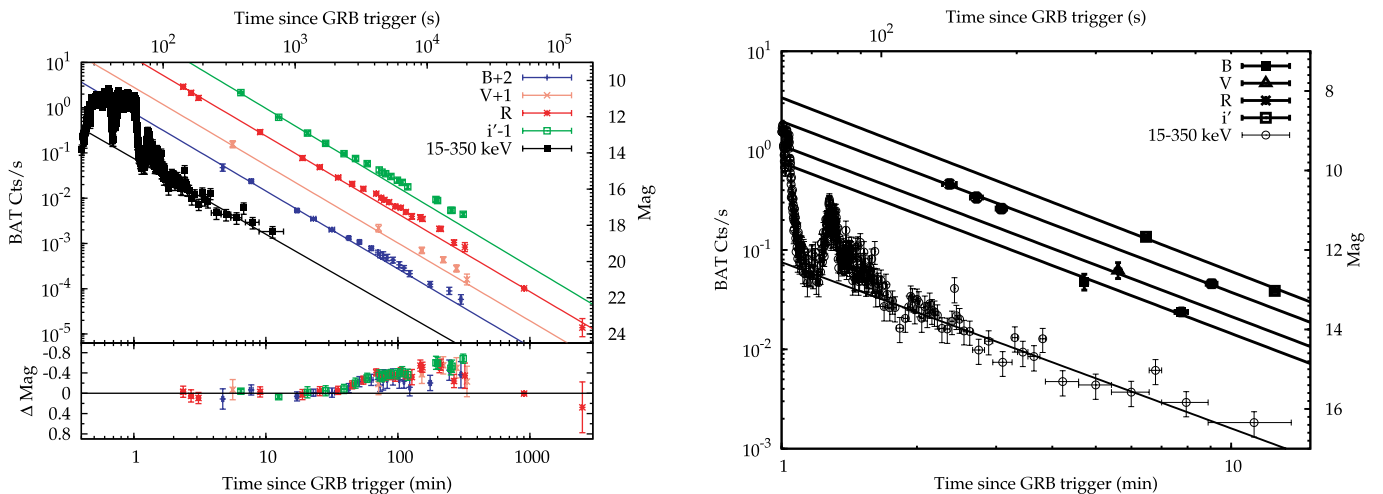

FIG. 1.—*Left:* FTS $BVRi'$ optical and *Swift* γ-ray light curves of GRB 061007. Optical light curves are fitted with a single power-law fits for $t < 40$ minutes, and the background-subtracted γ-ray light curve is fitted with a similar power law to data at $t > 120$ s. The BAT count rate (counts s^{-1} per fully illuminated detector for an equivalent on-axis source) and optical magnitudes are given on the left and right vertical axes, respectively. The bottom panel shows the optical residuals after removal of the corresponding power law (see Table 2), highlighting the presence of a broad bump in all filters for $t > 40$ minutes. Late-time R-band photometry from VLT and Magellan images are included at $t \sim 1000$ and $t \sim 2500$ minutes, respectively, and are consistent with extrapolation of the power-law decay. *Right:* An expanded view of the optical and γ-ray light curves at early time ($1 < t < 11$ minutes).

TABLE 2
RESULTS OF POWER-LAW FITS TO OPTICAL
AND γ-RAY LIGHT CURVES AS SHOWN IN FIG. 1

Band	Time Range For Fit	Temporal Power-Law Decay (α)
B	$t < 40$ minutes	1.72 ± 0.05
V	. . .	Fixed to α_R
R	$t < 40$ minutes	1.72 ± 0.01
i'	$t < 40$ minutes	1.75 ± 0.06
BAT (15–350 keV)	$t > 40$ s	1.7 ± 0.1

TABLE 3
BEST-FITTING PARAMETERS DERIVED FROM OPTICAL, X-RAY,
AND γ-RAY SPECTRAL ENERGY DISTRIBUTIONS

Parameter	SMC[a]	LMC	Milky Way	SMC, $\beta_{X\gamma}$ Fixed
β	1.02 ± 0.05	1.03 ± 0.05	1.03 ± 0.05	1.01
A_V (mag)......	0.48 ± 0.19	0.54 ± 0.20	0.54 ± 0.20	0.29 ± 0.06
χ^2/dof.........	$195/174$	$195/174$	$195/174$	$197/175$

[a] See Fig. 2.

in the 50–350 and 15–50 keV bands, which shows a marginal softening of the γ-ray spectrum with time.

3. RESULTS AND DISCUSSION

Figure 1 shows the FTS $BVRi'$ and background-subtracted *Swift*-BAT light curves of GRB 061007; a single power-law decay with $\alpha = 1.72 \pm 0.10$ ($F \propto t^{-\alpha}$) provides a good fit to all optical light curves for $t < 40$ minutes, resulting in small residuals in this time range and emphasizing the presence of an additional broad, multicolor bump over the time range $40 < t < 350$ minutes (see Table 2). Late-time VLT R-band photometry confirms that the underlying power-law decay continues, showing no evidence for a break before 1000 minutes (0.624 days). This is consistent with the continuation of the simple power-law decay in the XRT light curve (Schady et al. 2006b). Similarly, the marginal Magellan detection extends the continuation of the unbroken power-law decay to $t = 2495$ minutes (1.73 days), and, combined with the final upper limit $R > 23.3$ mag at 4087 minutes (2.84 days; Table 1), constrains the brightness of the host galaxy. A similar power law ($\alpha = 1.7 \pm 0.1$) also provides a good fit to the decay of the long, soft tail of the γ-ray emission for $t > 120$ s, although slight modulation of the power law due to the intrinsic variability is evident, as illustrated in the expanded view of the light curves of the first 10 minutes (Fig. 1, *right panel*; Table 2). A similar deviation
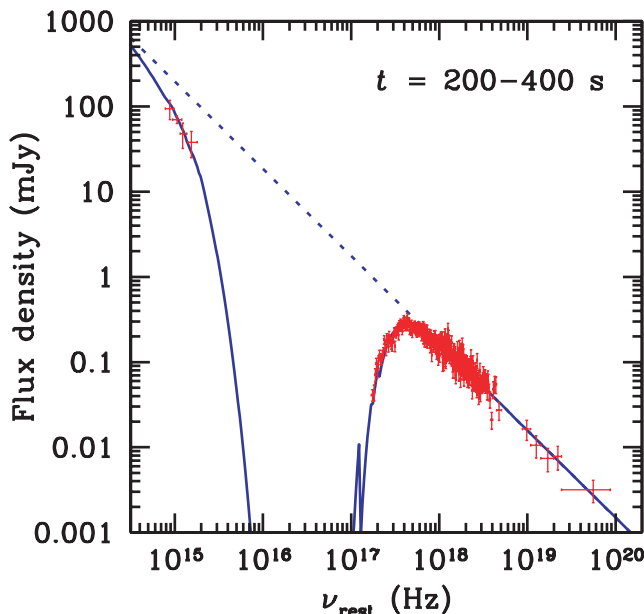
from the R-band power law may be present at ~ 2.3 minutes (see residuals Fig. 1), coincident in time with a small γ-ray flare, but the effect is marginal.

The broadband spectral energy distribution shown in Figure 2 confirms the overall common power-law decay in all bands from γ to optical and is well fitted by an absorbed power law with optical extinction $A_V \sim 0.48 \pm 0.19$ mag with an SMC profile. Comparing this with the N_H derived from the X-ray spectrum, we find a deficit of optical extinction, as already found in most GRBs (Stratta et al. 2004; Kann et al. 2006; Galama & Wijers 2001). In principle this could be explained in a number of ways (see, e.g., the case of GRB 051111, Guidorzi et al. 2007): (1) an extinction profile different from those typical of MW, SMC, LMC (e.g., Stratta et al. 2004; Savaglio & Fall 2004); (2) a population of dust grains skewed toward big sizes, possibly as a result of dust destruction due to the GRB itself (e.g., Maiolino et al. 2001; Chen et al. 2006); (3) a significant presence of molecular gas (1999); (4) overabundance of some alpha metals responsible for absorption in X-rays (e.g., GRB 050401; Watson et al. 2006).

Below, we explain the observed multiwavelength evolution of GRB 061007 at $t > 70$ s with an expanding fireball whose optical, X-ray, and γ-ray emission is dominated by synchrotron emission from a forward shock whose cooling frequency lies above the X-ray band and typical synchrotron frequency lies just below the optical band; in contrast, the typical frequency of the reverse shock lies in the radio band at early time, with the typical frequency of the forward shock entering the radio band at ~ 2.5 days after the burst.

3.1. Forward Shock Emission from a Decelerating Fireball

The optical and X-ray afterglow light curves are described by the same power law, $\alpha \sim 1.7$, to more than 10^5 s after the burst; this indicates that these photons are radiated from the same forward shock, and optical and X-ray bands are in the same domain
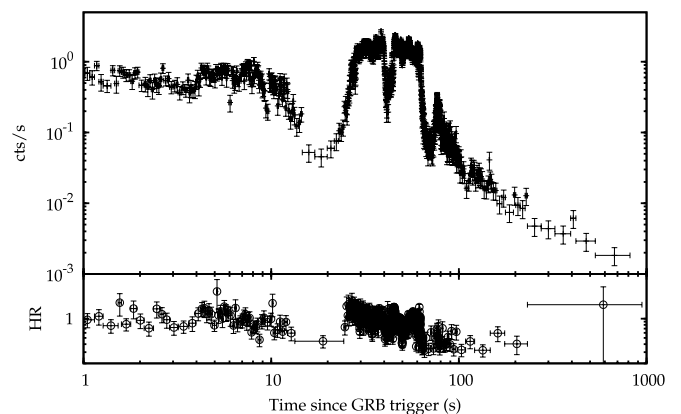

FIG. 2.—Broadband optical to γ-ray spectral energy distribution derived for the time interval $200 < t_{obs} < 400$ s, fitted with an absorbed power law with $\beta(\text{opt}, X, \gamma) = 1.02 \pm 0.05$ and rest-frame extinction $A_V(\text{SMC}) = 0.48 \pm 0.19$ mag (*solid line*). The unabsorbed power law is also shown (*dotted line*).

FIG. 3.— Evolution of the hardness ratio (HR), derived from comparison of count rates in 50–350 and 15–50 keV bands, compared with the BAT (15–350 keV), showing a marginal softening of the γ-ray spectrum with time.

of a synchrotron spectrum.[14] In principle a bump of a forward shock (blast wave) light curve, as seen for $t > 40$ minutes (Fig. 1), can be produced by inhomogeneity of the ambient medium or by energy injection into a blast wave. However, energy injection causes a transition from a blast wave to another with a larger energy, and it leads to a shift of the afterglow decay baseline after the bump (at this late time the evolution of a blast wave is adiabatic). Since the optical flux comes back to the prebump decay line, inhomogeneity of the ambient medium is favored to explain the bump around 100 minutes in the optical. The X-ray band (and the optical band) should be below the synchrotron cooling frequency ν_c, otherwise the inhomogeneity in the ambient medium does not produce an afterglow bump (Kumar 2000). For the synchrotron shock model, the decay index and spectral index at frequencies $\nu_m < \nu < \nu_c$ are $\alpha = 3(p-1)/4$ and $\beta = (p-1)/2$, respectively (Sari et al. 1998). With $p \sim 3$ these give reasonable fits to the observed indices. We note that if a burst occurred in a wind medium with density $n \propto R^{-s}$, the decay index in this spectral domain $\nu_m < \nu < \nu_c$ is given by $\alpha = [2s + 3(p-1)(4-s)]/(16-4s) \sim 1.7$ for $p = 3$ and $s = 1$ (Monfardini et al. 2006). The additional parameter s allows a better fits to the decay index, but still a rather large value of $p \sim 3$ is required to explain the observed β.

Since the optical and X-ray light curves show no break during the observations, the typical synchrotron frequency $\nu_m \propto t^{-3/2}$ should be already below the optical band $\nu_m < \nu_{\rm opt} \sim 5 \times 10^{14}$ Hz before our earliest optical observation was made at $t = 137$ s, while the cooling frequency $\nu_c \propto t^{-1/2}$ should be still above X-ray band $\nu_X < \nu_c \sim 10^{18}$ Hz at $t \sim 10^5$ s. Using the results in Sari et al. (1998), we get

$$\nu_m(t) \sim 1.0 \times 10^{21} \zeta^{1/2} \epsilon_B^{1/2} \epsilon_e^2 E_{54}^{1/2} t_m^{-3/2} \text{ Hz,} \tag{1}$$

$$\nu_c(t) \sim 6.8 \times 10^{12} \zeta^{-1/2} \epsilon_B^{-3/2} E_{54}^{-1/2} n^{-1} t_m^{-1/2} \text{ Hz,} \tag{2}$$

where $\zeta = (1+z)/2.26$, $E_{54} = E/10^{54}$ ergs, t_m is the observer's time in minutes, n is the density in cm^{-3}, ν_m is proportional to $(p-2)/(p-1)$, and we have assumed $p = 3$. The requirements for the break frequencies at $t = 137$ s and at $t = 10^5$ s give constraints on the microphysics parameters,

$$\epsilon_B < 3.0 \times 10^{-5} n^{-2/3} (\zeta E_{54})^{-1/3}, \tag{3}$$

$$\epsilon_e < 1.7 \times 10^{-2} \left(\frac{\epsilon_B}{3.0 \times 10^{-5}} \right)^{-1/4} (\zeta E_{54})^{-1/4}. \tag{4}$$

These energy partition values are somewhat small but are not inconsistent with values derived for other bursts (e.g., Panaitescu & Kumar 2002).

3.1.1. Onset of the Afterglow and Lack of Optical Flash

ROTSE detected a 13.6 mag optical counterpart at 26 s after the GRB trigger (Rykoff et al. 2006). This magnitude is dimmer than the extrapolation of our observations. It indicates that the afterglow peaked between 26 and 137 s, and very likely around the end of the main pulses of the prompt emission $t_p \sim 100$ s. Using this peak time, we can estimate the Lorentz factor of the fireball at that time (Sari & Piran 1999). It is

$$\Gamma \sim \left[\frac{3(1+z)^3 E}{32\pi n m_p c^5 t_p^3} \right]^{1/8} \sim 230 \left(\frac{t_p}{10^2 \text{ s}} \right)^{-3/8} (\zeta^3 E_{54}/n)^{-1/8}. \tag{5}$$

It is interesting that the tail of the γ-ray emission is described by the same power-law decay, $\alpha \sim 1.7$, as the optical and X-ray emission (Fig. 1); indeed, the flux at the dip in the prompt phase at ~ 40 s is consistent with the underlying power-law line. If the afterglow started at ~ 30 s, the Lorentz factor is ~ 360. No jet break[15] within 10^5 s gives a lower limit of the GRB jet opening angle $\theta_0(\text{rad}) > 0.07 n^{1/8} E_{54}^{-1/8} \zeta^{-3/8} (t/10^5 \text{ s})^{3/8}$.

There is no reverse shock emission component even though the optical observations started right after the prompt emission phase. We can explain the lack of optical flash naturally in the standard model if the typical frequency of the forward shock emission is lower than optical band $\nu_m < \nu_{\rm opt}$ at the onset of afterglow (the peak time t_p). At the peak time (the shock crossing time), the forward and reverse shocked regions have the same Lorentz factor and internal energy density, the cooling frequency of the reverse shock is equal to that of the forward shock $\nu_{c,r}(t_p) \sim \nu_c(t_p)$. The matter density in the reverse shocked region is much higher than in the forward shock region, and it makes the electron temperature lower. The typical frequency of the reverse shock is much lower than that of the forward shock $\nu_{m,r}(t_p) \ll \nu_m(t_p) < \nu_{\rm opt}$ (e.g., Kobayashi & Zhang 2003).

The shock regions have the same amount of shock energies at t_p, and their luminosities ($\sim \nu F_\nu$ at ν_c) are comparable at t_p. Considering that the two emission components have the same spectral index, at t_p they contribute equally to the flux at any observed frequency between $\nu_{m,f}$ and ν_c. After the shock crossing $t > t_p$ the reverse shock emission decays more rapidly as $\sim t^{-2}$, so the contribution from the reverse shock should be masked by the forward shock component in the decay phase.

Forward shock emission peaks when a fireball decelerates or when the typical frequency passes through the observed band. If an optical peak is not associated with a spectral change from $\nu^{1/3}$ to $\nu^{-(p-1)/2}$, it could be because of the deceleration of a fireball, and the typical frequency could be located below the observed band at that time. In such a case, the optical flash should always be absent. In recent years, ground-based robotic telescopes reported the lack of optical flashes, except for a few cases. The lack might be explained with low ν_m originating from rather small microphysics parameters, ϵ_e and ϵ_B. GRB 060117 and GRB 061007 might be clear example cases.

3.2. Implications for Late-Time Radio Emission

After the deceleration, the emission frequency of each electron in the shocked ejecta (reverse shock region) drops quickly with time as $\nu_e \propto t^{-73/48}$. Both the typical frequency and cooling frequency drop with this scaling, because after a reverse shock has crossed the ejecta (deceleration), no new electrons are injected and all electrons cool by adiabatic expansion only. The peak power decays as $F_{\nu, \max} \propto t^{-47/48}$. The flux below or above the typical frequency $\nu_{m,r}$ evolves as (Sari & Piran 1999; Kobayashi & Sari 2000, their eq. [3]),

$$F_\nu \propto \begin{cases} t^{-17/36}, & \nu < \nu_{m,r}, \\ t^{-(73p+21)/96} \propto t^{-5/2} (p=3), & \nu > \nu_{m,r}. \end{cases} \tag{6}$$

The optical afterglow of GRB 061007 was very bright. If the forward shock typical frequency is close to the optical band at the deceleration time $\nu_m(t_p) \sim 5 \times 10^{14}$ Hz, extrapolating our observational results to the deceleration time $t_p \sim 100$ s, we obtain the peak flux of the forward shock emission $F_{\nu, \max} \sim 420$ mJy. The

---

[14] Even if we assume reverse shock emission, the observed bands should be in the same spectral domain $\nu_m < \nu_{\rm opt}, \nu_X < \nu_c$, because reverse shock emission above the cooling frequency vanishes after the shock crossing. In this case we obtain the theoretical value $\alpha - 3\beta/2 \sim 1$ which is not consistent with observation $\alpha - 3\beta/2 \sim 0$.

[15] Another possible scenario is that a jet break happened immediately after the prompt phase at $t < 100$ s. This scenario requires a very small electron index to explain the decay indices of the optical and X-ray light curves.

typical frequency of the reverse shock emission is lower by a factor of $\sim \Gamma^2$ (Kobayashi & Zhang 2003), and it is in the radio band $\nu_{m,r}(t_p) \sim \nu_m/\Gamma^2 \sim 9.5(\Gamma/230)^{-2}$ GHz. At the deceleration time, the peak flux of the reverse shock emission is larger by a factor of $\Gamma \sim 230$ than that of the forward shock emission. Since the reverse shock emission in the radio band initially decays as $t^{-17/36}$ until the typical frequency passage, then as $t^{-5/2}$, the reverse shock radio emission at 1 day is about $\sim 8.6(\nu/4.8 \text{ GHz})^{-1}(t/1 \text{ day})^{-5/2}$ μJy.

The typical frequency of the forward shock emission $\nu_m \propto t^{-3/2}$ comes to radio band $\nu = 4.8$ GHz about 2.5 days after the burst. Before the passage, the flux increases as $t^{1/2}$, and then decays as $t^{-1.7}$. The peak value is expected to be ~ 420 mJy. At low frequencies and early times, self-absorption plays an important role and significantly reduces the afterglow flux. A simple rough estimate of the maximum flux is the emission from a blackbody with the shock temperature (e.g., Sari & Piran 1999; Kobayashi & Sari 2000). The temperature is given by the random energy of the typical electron $k_B T \sim m_e c^2 \gamma_m \sim \epsilon_e m_p c^2 \Gamma/2$ for $p = 3$. If the observed frequency is above the typical frequency, the electrons radiating into the observed frequency have an energy higher than the typical energy, $m_e c^2 \gamma_m$, by a factor of $(\nu/\nu_m)^{1/2}$. Following the notation of Sari & Piran (1999), the upper limit of blackbody emission is

$$F_\nu^{\text{BB}} = \pi(R_\perp/d)^2 \Gamma S_\nu, \qquad (7)$$

where $d = d_L/(1+z)^{1/2}$ and $S_\nu = (2\nu^2/c^2)k_B T$. Therefore,

$$F_\nu^{\text{BB}} \sim \pi(1+z)m_p \nu^2 \epsilon_e \Gamma^2 \left(\frac{R_\perp}{d_L}, 2\right) \qquad (8)$$

$$\sim 6\left(\frac{\nu}{4.8 \text{ GHz}}\right)^2 \left(\frac{t}{1 \text{ day}}\right)^{1/2} \epsilon_{e,-2}(E_{54}/n)^{1/2} \text{ mJy}, \qquad (9)$$

where $\epsilon_{e,-2} = \epsilon_e/10^{-2}$ and $R_\perp \sim 4.6\Gamma ct$ is the observed size of the fireball, assuming $z = 1.26$ and $d_L = 2.7 \times 10^{28}$ cm. Note that other emission estimates use only scalings (normalizations are given by the observations), the blackbody upper limit is more model dependent.

The results from ATCA (van der Horst & Rol 2006a, 2006b) give even lower limits about 50 μJy level. Their formal flux measurements are -25 ± 45 μJy (1.00–1.24 days after the burst) and -1 ± 43 μJy (5.03–5.28 days after) at 4.8 GHz. Although the blackbody limit is possibly less reliable, the radio nondetection might imply a high-density environment $n \gg 1$. The peak flux of the forward shock emission is given by (Sari et al. 1998)

$$F_{\nu,\text{max}}(z = 1.26) \sim 20\left(\frac{\epsilon_B}{5 \times 10^{-5}}\right)^{1/2} E_{54}n^{1/2} \text{ mJy}. \qquad (10)$$

As can be seen from equations (3) and (10), the dependence of $F_{\nu,\text{max}}$ on density is weak ($\sim n^{1/6}$), and thus the bright afterglow cannot be easily explained by a high-density environment.

3.3. GRB 061007 and Cosmological Spectral Energy Correlations

Swift GRB 061007 is one of the most luminous GRBs ever detected, and thus, with its high-quality γ-ray data, well-characterized light curves and well-determined peak energy, it is an ideal object to test the cosmological spectral energy correlations, namely,

the E_{peak}-E_{iso} (Amati et al. 2002), E_{peak}-E_γ (Ghirlanda et al. 2004) and E_{peak}-E_{iso}-t_b (Liang & Zhang 2005) correlations. As described in § 2, the prompt γ-ray emission at Mev energies was detected by three additional satellites that provide estimates of the peak energy. While the peak energies measured by Konus-*Wind* and *RHESSI* are comparable, that measured by *Suzaku* WAM is significantly larger; in addition to possible systematics, this may be explained by the fact that this instrument measured the brightest part of the GRB, as suggested by their low duration estimate ($T90 \sim 50$ s vs. 90 s measured by Konus-*Wind*).[16] We therefore use the spectral information from Konus-*Wind* and *RHESSI*, conservatively assuming an E_{peak} range including both 90% c.l. intervals provided by the two instruments, i.e., $E_{\text{peak}} = 394 \pm 55$ keV, corresponding to a cosmological rest-frame peak energy of 890 ± 124 keV.

The isotropic–equivalent radiated energy is $E_{\text{iso}} = (1.0 \pm 0.1) \times 10^{54}$ ergs in the 1–10,000 keV cosmological rest frame, assuming $H_0 = 70$ km s^{-1} Mpc^{-1}, $\Omega_\Lambda = 0.3$, and $\Omega_m = 0.7$ and a Band spectral shape (Band et al. 1993) with parameters and fluence provided by Konus-*Wind* (Golenetskii at al. 2006. Following Amati (2006) the E_{peak}-E_{iso} correlation predicts a corresponding $E_{\text{peak}} = 907$ keV, fully consistent with the measured value for GRB 061007. Thus, GRB 061007 further confirms the validity of the E_{peak}-E_{iso} correlation in the very high radiated energy regime, and since this correlation should only hold for prompt emission, confirms that GRB 061007 has prompt emission typical of other *Swift* bursts on the correlation, despite its unusually simple afterglow emission.

Finally, the test of the E_{peak}-E_γ and E_{peak}-E_{iso}-t_b correlations, which is of particular importance given their possible use for the estimate of cosmological parameters (e.g., Firmani et al. 2006), requires the detection of a late break in the afterglow light curves. As can be seen in Figure 1, our optical light curves show no evidence of a break up to ~ 150 ks, and the XRT light curve continues unbroken to at least 10^6 s (Schady et al. 2006b), providing a firm lower limit to the jet break time. Combining our estimates of E_{iso} and the lower limit to the jet opening angle of $\sim 4.7°$ inferred from the optical light curve, we derive a collimation-corrected energy $E_\gamma > 3.4 \times 10^{51}$ ergs; this limit would predict $E_{\text{peak}} > 1274$ keV in order to be consistent with the E_{peak}-E_γ correlation (Nava et al. 2006), a value somewhat higher than the measured value of 890 ± 124 (90% c.l.). By accounting for the logarithmic dispersion of this correlation (Nava et al. 2006), the deviation of the measured value from this lower limit is $\sim 1.6 \sigma$. Better consistency is found with the E_{peak}-E_{iso}-t_b correlation, which, when adopting the parameters reported by Liang & Zhang (2005), predicts a lower limit to E_{peak} of 986 keV. Using the lower limit to the jet break time $t \sim 10^6$ s suggested by the X-ray light curve, we conclude that GRB 061007 becomes a secure outlier to both E_{peak}-E_γ and E_{peak}-E_{iso}-t_b correlations, deviating by more than 3σ. X-ray light curves for other GRBs suggest the existence of a population of objects similar to GRB 061007 that are inconsistent with these correlations (Sato et al. 2006; Willingdale et al. 2006), although optical observations were not available for these objects. GRB 061007 might therefore transpire to be the norm rather than an anomaly.

4. CONCLUSIONS

We have presented a multiwavelength study of the very bright GRB 061007 based on optical observations that cover the period

---

[16] The lower bound of the energy band of WAM is somewhat higher than that of Konus-*Wind* and *RHESSI*, which may result in an overestimate of E_{peak} (Amati 2006).

from 137 s to 3 days after the burst and *Swift* XRT and BAT data. We conclude that the afterglow commences as early as 30–100 s after the onset of the GRB and the optical, X-ray, and underlying γ-ray emission, which are described by the same power-law decay, $\alpha \sim 1.7$, after this time, represent photons that are radiated from the same forward shock, with optical and X-ray bands in the same domain of a synchrotron spectrum. In contrast, the typical frequency of the reverse shock emission is already in the radio domain at early time, explaining the lack of a bright early-time optical flash and late time radio flare. We note the similarity of the light curves of GRB 061007 to that of GRB 060117, which was only observed in a single optical filter (Jelínek et al. 2006) and suggest it too may represent the onset of an early afterglow similar to GRB 061007. Finally, we highlight the simplicity of the early-onset afterglow of GRB 061007, which with its well-behaved light curves, typical circumburst environment, and well-determined peak γ-ray energy, make it a useful candidate for inclusion in current cosmological correlations. We find that this event is fully consistent within 1 σ with the $E_{\rm peak}$-$E_{\rm iso}$ correlation and also potentially consistent within 1.6 σ with the $E_{\rm peak}$-E_γ and

$E_{\rm peak}$-$E_{\rm iso}$-t_b correlations using a lower limit to the jet break time t_b, and thus to E_γ, derived from our data. We note that since the X-ray afterglow continued without a jet break until $t > 10^6$ s, this event is firm outlier to the $E_{\rm peak}$-E_γ and $E_{\rm peak}$-$E_{\rm iso}$-t_b correlations, deviating from these correlations by more than $\sim 3 \sigma$.

REFERENCES

Akerlof, C., et al. 1999, Nature, 398, 400
Amati, L. 2006, MNRAS, 372, 233
Amati, L., et al. 2002, A&A, 390, 81
Band, D., et al. 1993, ApJ, 413, 281
Bersier et al. 2006, GCN Circ. 5709, http://gcn.gsfc.nasa.gov/gcn/gcn3/5709.gcn3
Boër, M., Atteia, J. L., Damerdji, Y., Gendre, B., Klotz, A., & Stratta, G. 2006, ApJ, 638, L71
Burrows, D. N., et al. 2006, in The X-Ray Universe 2005, Vol. 2, ed. by, A. Wilson (ESA SP-604; Noordwijk: ESA). 877
Cardelli, J. A., Clayton, G. C., & Mathis, J. S. 1989, ApJ, 345, 245
Chen, S. L., Li, A. G., & Wei, D. M. 2006, ApJ, 647, L13
Dai, X., Halpern, J. P., Morgan, N. D., Armstrong, E., Mirabal, N., Haislip, J. B., Reichart, D. E., & Stanek, K. Z. 2007, ApJ, in press (astro-ph/0609269)
Firmani, C., Ghisellini, G., Avila-Reese, V., & Ghirlanda, G. 2006, MNRAS, 370, 185
Fukugita, M., et al. 1996, AJ, 111, 1748
Galama, T. J., & Wijers, A. M. J. 2001, ApJ, 549, L209
Gehrels, N., et al. 2004, ApJ, 611, 1005
Ghirlanda, G., Ghisellini, G., & Lazzati, D. 2004, ApJ, 616, 331
Golenetskii, S., Aptekar, R., Mazets, E., Pal'Shin, V., Frederiks, D., & Cline, T. 2006, GCN Circ. 5722, http://gcn.gsfc.nasa.gov/gcn/gcn3/5722.gcn3
Gomboc et al. 2007, Nuovo Cimento, in press (astro-ph/0612762)
Guidorzi, C., et al. 2005, ApJ, 630, L121
———. 2006a, PASP, 118, 288
———. 2007, A&A, 463, 539
Heyl, J. S., & Perna, R. 2003, ApJ, 586, L13
Jakobsson, P., et al. 2006, GCN Circ. 5716, http://gcn.gsfc.nasa.gov/gcn/gcn3/5716.gcn3
Jelínek, M., et al. 2006, A&A, 454, L119
Kalberla, P. M. W., Burton, W. B., Hartmann, D., Amal, E. M., Bajaja, E., Morras, R., & Pöppel, W. G. L. 2005, A&A, 440, 775
Kann, D. A., Klose, S., & Zeh, A. 2006, ApJ, 641, 993
Kobayashi, S. 2000, ApJ, 545, 807
Kobayashi, S., & Sari, R. 2000, ApJ, 542, 819
Kobayashi, S., & Zhang, B. 2003, ApJ, 582, L75
Kumar, P. 2000, ApJ, 538, L125
Kumar, P., & Piran, T. 2000, ApJ, 532, 286
Lazzati, D., Rossi, E., Covino, S., Ghisellini, G., & Malesani, D. 2002, A&A, 396, L5
Liang, E., & Zhang, B. 2005, ApJ, 633, 611
Maiolino, R., Marconi, A., & Oliva, E. 2001, A&A, 365, 37
Markwardt, C., et al. 2006, GCN Circ. 5713, http://gcn.gsfc.nasa.gov/gcn/gcn3/5713.gcn3
Melandri, A., et al. 2007, in AIP Conf. Proc., The Multicolored Landscape of Compact Objects, ed. L. Burderi et al. (Melville: AIP), in press

Monfardini, A., et al. 2006, ApJ, 648, 1125
Mundell, C., et al. 2006, GCN Circ. 5708, http://gcn.gsfc.nasa.gov/gcn/gcn3/5708.gcn3
Nakar, E., & Piran, T. 2005, ApJ, 619, L147
Nakar, E., Piran, T., & Granot, J. 2003, NewA, 8, 495
Nava, L., Ghisellini, G., Ghirlanda, G., Tavecchio, F., & Firmani, C. 2006, A&A, 450, 471
Oates, S., et al. 2006, MNRAS, 372, 327
O'Brien, P., et al. 2006, ApJ, 647, 1213
Osip, D., et al. 2006, GCN Circ. 5715, http://gcn.gsfc.nasa.gov/gcn/gcn3/5715.gcn3
Panaitescu, A. and Kumar, P. 2002, ApJ, 571, 779
Pei, Y. C. 1992, ApJ, 395, 130
Romano, P., et al. 2006, A&A, 456, 917
Roming, P., et al. 2006, ApJ, 652, 1416
Rykoff et al. 2006, GCN Circ. 5706, http://gcn.gsfc.nasa.gov/gcn/gcn3/5706.gcn3
Sari, R., & Mészáros, P. 2000, ApJ, 535, L33
Sari, R., & Piran, T. 1999, A&AS, 138, 537
Sari, R., Piran, T., & Narayan, R. 1998, ApJ, 497, L17
Sato, G., et al. 2006, ApJ, in press
Savaglio, S., & Fall, S. M. 2004, ApJ, 614, 293
Schady, P., & Pandy, S. 2006, GCN Circ. 5719, http://gcn.gsfc.nasa.gov/gcn/gcn3/5719.gcn3
Schady, P., et al. 2006a, GCN Circ. 5707, http://gcn.gsfc.nasa.gov/gcn/gcn3/5707.gcn3
Schady et al. 2006b, MNRAS, submitted (astro-ph/0611081)
Schlegel, D. J., Finkbeiner, D. P., & Davis, M. 1998, ApJ, 500, 525
Stanek, K. Z., et al. 2007, ApJ, 654, L21
Stratta, G., Fiore, F., Antonelli, L. A., Piro, L., & de Pasquale, M. 2004, ApJ, 608, 846
van der Horst, A. J., & Rol, E. 2006a, GCN Circ. 5720, http://gcn.gsfc.nasa.gov/gcn/gcn3/5720.gcn3
———. 2006b, GCN Circ. 5726, http://gcn.gsfc.nasa.gov/gcn/gcn3/5726.gcn3
Vetere, L., et al. 2006, GCN Circ. 5712, http://gcn.gsfc.nasa.gov/gcn/gcn3/5712.gcn3
Watson, D., et al. 2006, ApJ, 652, 1011
Wigger, C., et al. 2006, GCN Circ. 5725, http://gcn.gsfc.nasa.gov/gcn/gcn3/5725.gcn3
Willingdale, R., et al. 2006, ApJ, submitted (astro-ph/0612031)
Wozniak, P. R., Vestrand, J. A., Wren, J. A., White, R. R., Evans, S. M., & Casperson, D. 2006, ApJ, 642, L99
Yamaoka, K., et al. 2006, GCN Circ. 5724
Zhang, B., & Mészáros, P. 2002, ApJ, 566, 712